IEEE Access
Multidisciplinary ⋮ Rapid Review ⋮ Open Access Journal

Received 6 September 2023, accepted 25 October 2023, date of publication 2 November 2023,
date of current version 13 November 2023.

Digital Object Identifier 10.1109/ACCESS.2023.3329512

RESEARCH ARTICLE

Multi-Beam 5G Antenna With Miniaturized Butler Matrix Using Stacked LTCC

JAEWOONG JUNG[1], JONGIN RYU[2], (Member, IEEE), AND KYUNG-YOUNG JUNG[1], (Senior Member, IEEE)

[1]Department of Electronic Engineering, Hanyang University, Seoul 04763, South Korea
[2]Package Research Center, Korea Electronics Technology Institute, Seongnam, Gyeonggi-do 13509, South Korea

Corresponding author: Kyung-Young Jung (kyjung3@hanyang.ac.kr)

This work was supported by the Institute of Information and Communications Technology Planning and Evaluation (IITP) Grant funded by the Korea Government (MSIT) (Development of ultra-precision low-cost sub-THz pulse-based radar chip technology) under Grant 2022-0-01016.

ABSTRACT In this work, we present a compact four-direction beamforming 5G antenna based on a stacked 4 × 4 Butler matrix and a microstrip patch array antenna. The proposed beamforming antenna is a stacked-up structure using the low temperature co-fired ceramics (LTCC) process and thus its size can be significantly reduced by compared to a conventional beamforming antenna with a single-layer 4 × 4 Butler matrix. Moreover, spurious radiation generated from the Butler matrix can be effectively suppressed due to shielding effects inherent to the multilayer substrate. The fabricated beamforming antenna is composed the stacked 4 × 4 Butler matrix with striplines and the 4 × 1 array microstrip patch antenna. The overall size of the fabricated antenna system is 22.02 mm × 5.93 mm × 1.20 mm. The beam steering angles are measured to be −16°, 45°, −45° and 16°.

INDEX TERMS Butler matrix, array patch antenna, beamforming network, stacked butler matrix, 5G.

I. INTRODUCTION

In the realm of 5G communication systems, the integration of beamforming network-based antennas is essential to optimize data rates and maximize access point density [1], [2], [3], [4], [5], [6], [7], [8], [9]. Typically, two approaches are available for implementing the beamforming network system. The first approach entails an adaptive beamforming network capable of continuous beam steering in any direction. However, this method incurs high implementation costs and involves design complexities [10]. In contrast, a passive beam-forming network offers an alternative solution with reduced hardware complexity and cost, while still enabling beam steering capabilities in a discontinuous manner. Various passive beamforming matrices, including the Blass matrix [11], [12], Nolean matrix [13], Rotman lens [14], [15], and Butler matrix [16], [17], [18], [19], [20], are utilized in the switched beamforming antenna system. Among these alternatives, the Butler matrix has attracted significant attention due to its straightforward implementation and low power dissipation.

The associate editor coordinating the review of this manuscript and approving it for publication was Wanchen Yang.

However, it is worth noting that the Butler matrix generally occupies a larger area compared to the array antenna within the beamforming antenna system. Therefore, minimizing the size of the Butler matrix is crucial in reducing the overall size of the beamforming antenna system. This is particularly important in contemporary, space-limited applications such as IoT devices, mobile devices, and sensor networks [21], [22].

Consequently, the development of a miniaturized Butler matrix holds utmost significance in meeting industry requirements. The miniaturization techniques for the Butler matrix can be categorized into two main approaches: single-layer design and multilayer design. The single-layer design employs methodologies such as the utilization of lumped elements in a coupler [23] and meander transmission lines [24]. While these techniques effectively achieve mini-aturization, they can suffer from the problem of spurious radiation leakage from the Butler matrix, as it coexists with the array antenna on the same layer. This phenomenon can significantly impact the overall radiation pattern and compromise the antenna's performance.

On the other hand, the dual-layer design offers an alternative solution. Several studies in the literature have explored this approach [25], [26], [27], [28]. In [25] and [26], a modified Butler matrix is located on the bottom layer and the array antenna is placed on the top layer. In [27], the dual-layer Butler matrix is designed to implement the cross-over circuit and the array antenna is located on the top layer. In [28], the authors implemented the Butler matrix based on a substrate integrated waveguide (SIW) and placed the array antenna on the SIW. In [29], the dual-layer Butler matrix is designed on the SIW technology and the array antenna is placed on the SIW. Note that the dual-layer design can miniaturize the Butler matrix and simultaneously alleviate spurious radiation effects.

However, to achieve further size reduction and eliminate the spurious radiation effects, it is essential to partition the Butler matrix antenna into finer subcomponents and arrange them in a vertical stack. Furthermore, the selection of a high dielectric constant as a substrate is necessary to achieve greater size reduction.

In this paper, we propose a beamforming antenna system for 5G communication, utilizing a stacked 4 × 4 Butler matrix implemented in low-temperature co-fired ceramics (LTCC). The incorporation of LTCC, with its high dielectric constant of 7.5, enables a compact design. Furthermore, LTCC exhibits favorable manufacturing characteristics for multilayer structures, as it is compatible with printing and filling processes using conductive silver paste. The proposed beamforming antenna system divides the Butler matrix antenna into four subcomponents and vertically stack them. Atop this assembly, an array patch antenna is positioned. Although patch antennas are identified with bandwidth as a limitation, their notable attributes lie in their low profile and seamless compatibility with integrated circuits, making them a favorable choice, especially for our work where space efficiency is paramount. By adopting this design strategy, we have realized not just a notable miniaturization but also a significant reduction in spurious radiation effects. This approach can achieve significant size reduction and eliminate spurious radiation effects. The remainder of this paper is organized as follows. We first present the components of the 4 × 4 Butler matrix, which are designed using LTCC-based stripline technology. Next, we propose the stacked configuration for the 4 × 4 Butler matrix, where the components are vertically stacked in four layers. In addition, we present the integration of the stacked Butler matrix with the LTCC-based patch array antenna. Also, the effects of the spurious radiation are investigated. To validate the design, the proposed Butler matrix antenna is fabricated and experimental results are presented. Finally, concluding remarks are provided.

II. DESIGN & ANAYLSIS

A. COMPONENTS OF STACKED 4 × 4 BUTLER MATRIX

This section begins by presenting the structure of a conventional 4 × 4 Butler matrix. Subsequently we introduce a novel design that illustrates the vertical stacking configuration of the proposed Butler matrix components.

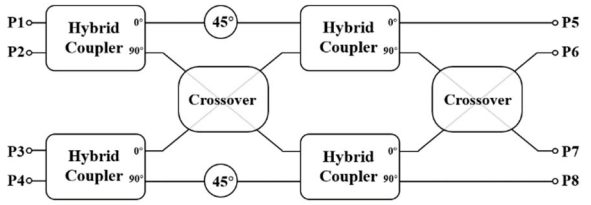

FIGURE 1. Schematic of the conventional 4 × 4 Butler matrix.

Fig 1 illustrates the structure of a typical 4 × 4 Butler matrix, which consists of four hybrid couplers, two crossovers, and two 45° delay lines. The 4 × 4 Butler matrix incorporates four input ports (P1−P4) and four output ports (P5−P8). The output ports of the Butler matrix are connected to an array antenna. Upon exciting one of the input ports, the Butler matrix produces four output signals with equal power but varying phase characteristics.

In this work, we propose a novel approach to partition the 4 × 4 Butler matrix antenna into smaller subcomponents and arrange them in a vertical stack. Fig. 2(a) depicts the proposed structure, which consists of four stages labeled A to D. Stage A and C consist of two 3 dB hybrid couplers each, while Stage B includes one 0 dB crossover and two 45° delay lines. Stage D consists of one 0 dB crossover and two full wavelength lines. As shown in Fig. 2(b), these

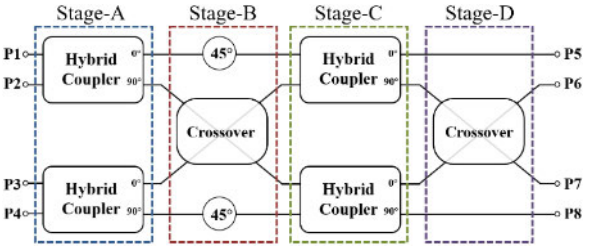

(a)

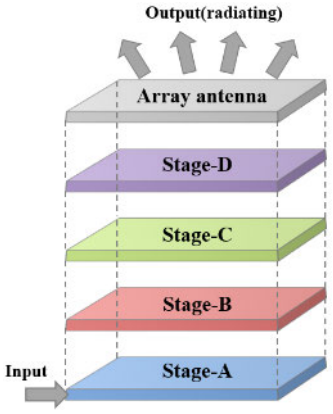

(b)

FIGURE 2. (a) Schematic of the 4 × 4 Butler matrix with four stages. (b) Topology of the stacked 4 × 4 Butler matrix antenna.

stages are vertically stacked, with the array antenna located on the top layer. All subcomponents of the Butler matrix, including the hybrid couplers, crossovers, and delay lines, are imple-mented using striplines. The feeding of the array antenna from the Butler matrix can be achieved either via or aperture-coupling methods. In our design, the via feeding method was chosen due to its ease of implementation using the LTCC process. Moreover, all layers in Stage A to D are interconnected through vias.

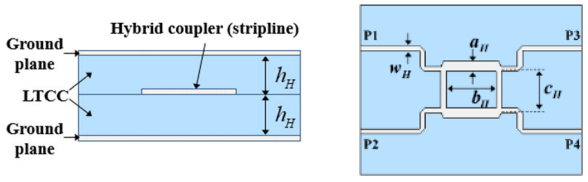

FIGURE 3. (a) Cross-sectional view of the 3dB hybrid coupler with stripline. (b) Top view of the 3 dB hybrid coupler.

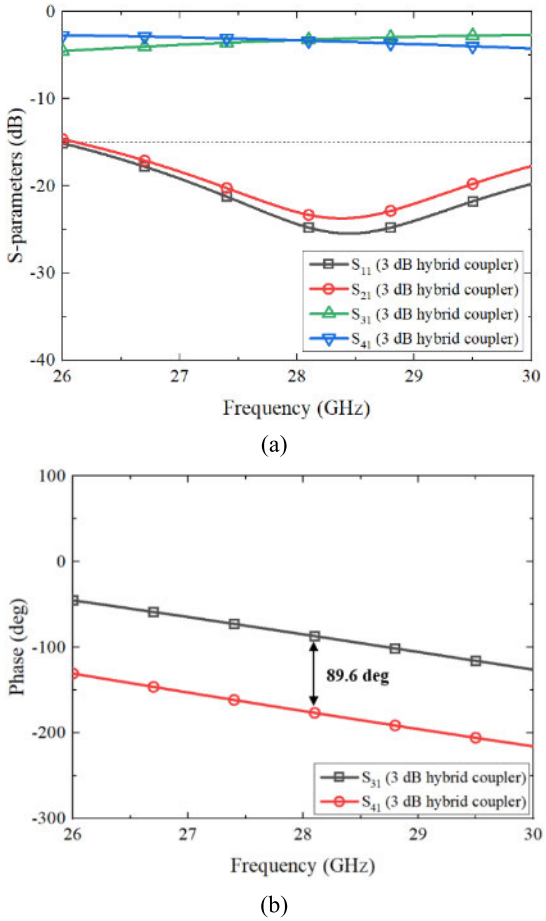

FIGURE 4. (a) Simulated S-parameters of the 3 dB hybrid coupler. (b) Simulated output phase difference of the 3 dB hybrid coupler.

Having discussed the proposed partitioning and stacking approach of the Butler matrix, we now delve into the key components that contribute to its functionality. The hybrid coupler plays a critical role in the functionality of the Butler matrix by uniformly distributing power and introducing a 90° phase delay. Fig. 3 provides the cross-sectional and top views of the hybrid coupler, illustrating its stacked structure utilizing the stripline configuration with ground planes on both the top and bottom layers, as depicted in Fig. 3(a). Fig. 4 presents the simulated S-parameters and phase results of the designed hybrid coupler. In Fig. 4(a), it can be observed that the reflection and isolation levels are below −15 dB within the frequency range of 26.1 GHz to 30 GHz. Moreover, the proposed hybrid coupler exhibits transmission coefficients of −3.27 dB from P1 to P3 and P4, indicating successful equal power distribution. The phases from P1 to P3 and P4 are depicted in Fig. 4(b), illustrating a phase difference ($\angle S_{31}-\angle S_{41}$) between P3 and P4 ranging from 85° to 90° across the frequency range of 26 GHz to 30 GHz.

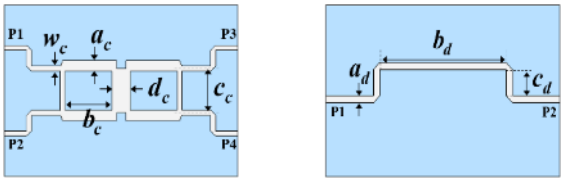

FIGURE 5. Top view of (a) 0 dB crossover and (b) 45 ° delay line.

Fig. 5 shows the configuration a 0 dB crossover and a 45° delay line. The 0 dB crossover facilitates the transfer of input power without introducing any phase delay, resulting in equal output power, as shown Fig. 5(a). The 45° delay line configuration, as depicted in Fig. 5(b), plays a crucial role in introducing a specific phase delay of 45° to the signal. Fig. 6(a) illustrates that the 0 dB crossover exhibits reflection and isolation levels falling below −15 dB within the frequency range of 27.1 GHz to 30 GHz. The 0 dB crossover has been verified to have the transmission coefficient of approxi-mately −0.3 dB from the input port to the output port, ensuring no power distribution. Fig. 6(b) displays the phases response of the 0 dB crossover and the 45° delay line. The transmission coefficient phase $\angle S_{41}$ of the 0 dB crossover has the phase of about 0° and the transmission coefficient phase $\angle S_{21}$ of the 45° delay line approaches 45° at 28 GHz. The all parameters of the designed components were optimized using the CST Studio Suite simulation tool, and the resulting optimized parameters are summarized in Section III.

B. STACKED BUTLER MATRIX ANTENNA MODULE

The stacked 4 × 4 Butler matrix is now implemented by integrating all relevant components as depicted in Fig. 7. It utilizes a vertical stacked structure comprising five layers: four layers for incorporating the previously described Butler matrix components and one layer for coplanar waveguide with ground (CPWG) feeding. Organized into four stages, as depicted in Fig. 8, each stage sequentially arranges the Butler matrix components. Additionally, shielding vias (SV)

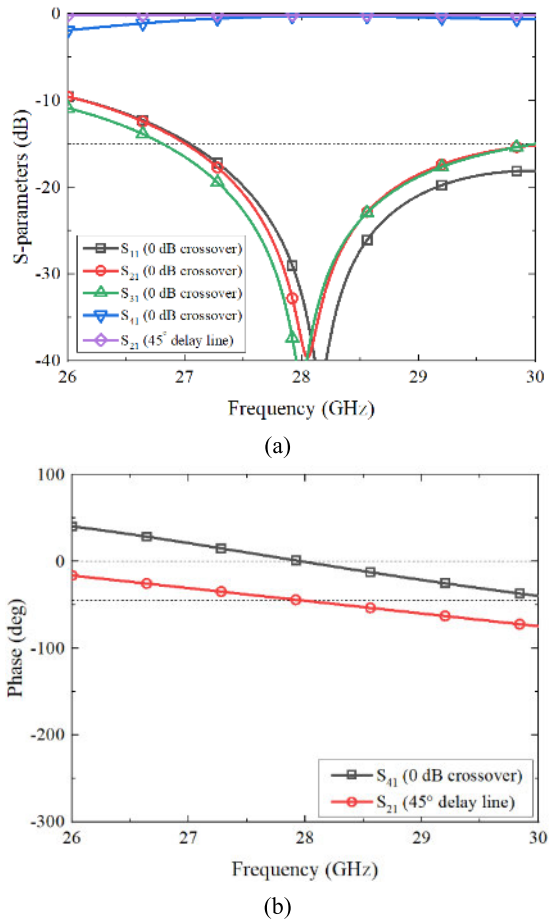

FIGURE 6. (a) Simulated S-parameters of the 0 dB crossover. (b) Simulated phase of the crossover and 45° delay line.

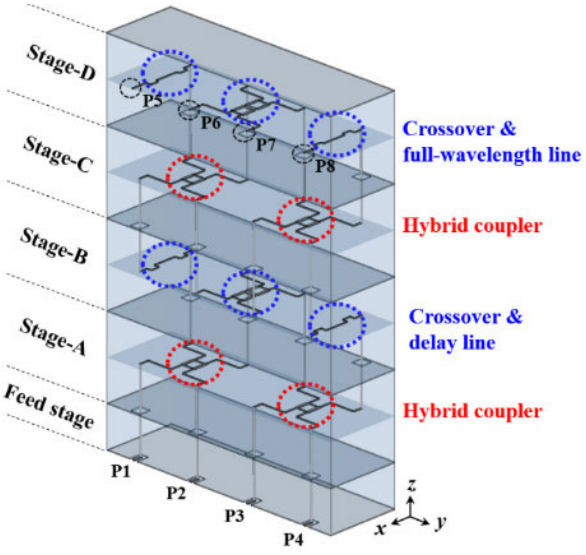

FIGURE 7. Total layout of the stacked 4 × 4 Butler matrix.

are strategically positioned in each stage to mitigate leakage energy generated from the through-via. Stage A and Stage C consist of two hybrid couplers, while Stage B incorporates a single crossover and two 45° phase delay lines.

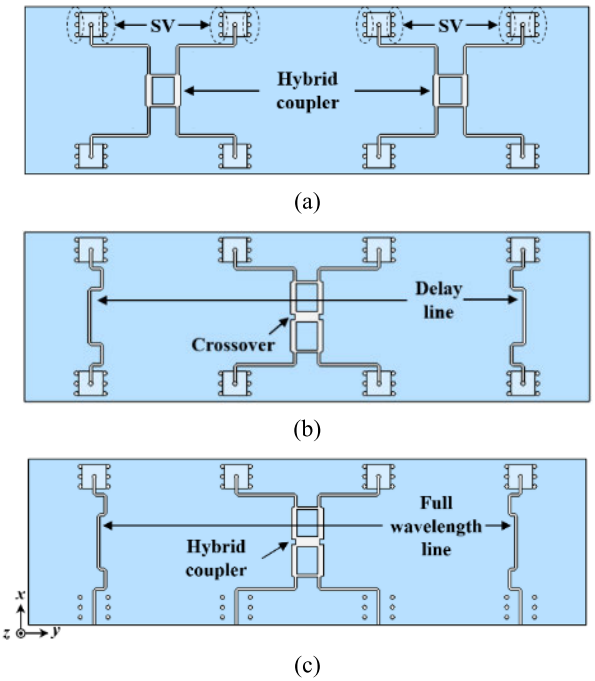

FIGURE 8. Structure of the stacked 4 × 4 Butler matrix. (a) Stage A, Stage C. (b) Stage B. (c) Stage D.

Furthermore, Stage D includes one 0 dB crossover and two full wavelength transmission lines. Fig. 9 illustrates the cross-sectional view of the stacked 4 × 4 Butler matrix in the x–z plane. The bottom layer consists of a feed stage with a CPWG, designed for assembly on a test board for measurements. The input signals of P1−P4 are transferred sequentially from the feed stage to the vertically stacked Stage A−D using through-via with a diameter of 0.15 mm ($\emptyset d_s$). To prevent short-circuits between the through-vias and the ground layers (G2–G5), anti-pads are implemented. As described in Section II, the input impedance of each component is designed to be characteristic impedance of 50 Ω. However, an impedance mismatch point (MMP) arises when connecting the through-via to each stage due to the higher impedance of the through-via compared to the stripline. Therefore, a solution is necessary to address the MMP issue. Fig. 10 illustrates the three-dimensional structure and cross-sectional view in the x–z plane of the MMP. To achieve impedance matching between the stage's transmission line and the through-via, the capacitance of the through-via needs to be adjusted, which depends on the distance between the trough-via and the middle ground. Specifically, the width of anti-pad (a_s) should be optimally set, and the simulated reflection coefficients according to a_s are shown in Fig. 11. The results demonstrate that when a_s is 0.8 mm, the reflection coefficient is the lowest in the frequency range of 26 GHz to 30 GHz. Based on these results, the optimized value of a_s obtained from the simulations was applied to the MMP of the stacked 4 × 4 Butler matrix.

Fig. 12 presents the simulated S-parameters of the 4 × 4 stacked Butler matrix with excitation at input

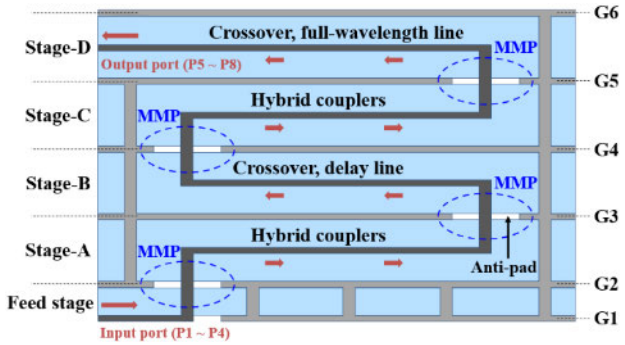

FIGURE 9. Cross-sectional view in the x–z plane of the stacked 4 × 4 Butler matrix.

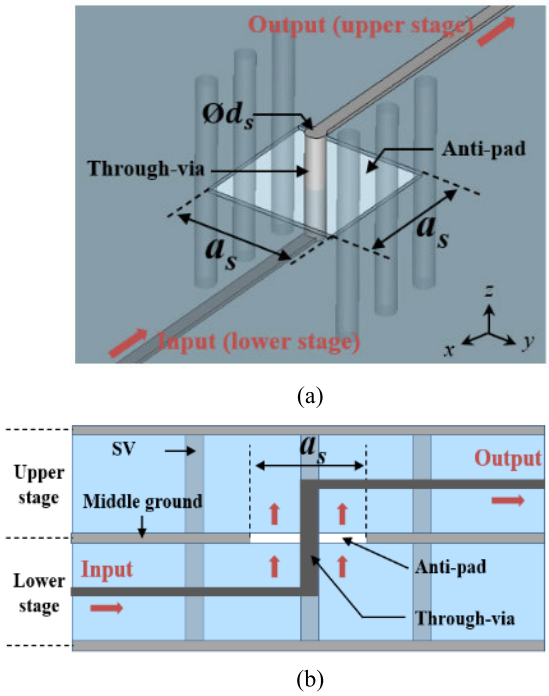

FIGURE 10. (a) Structure of the MMP in a three-dimensional. (b) Cross-sectional view of the MMP in the x–z plane.

ports P1 and P2. When P1 is excited, as shown in Fig 12(a), the reflection and isolation levels remain below −15 dB in the frequency range of 26.7 GHz to 28.5 GHz. At 28 GHz, the simulated transmission coefficients from P1 to output ports P5−P8 are −7.72 dB, −8.01 dB, −9.44 dB, and −8.87 dB, respectively. Similarly, when P2 is excited, as depicted in Fig 12(b), the reflection and isolation levels are below −15 dB over the frequency range of 27.2 GHz to 28.5 GHz. At 28 GHz, the simulated transmission coefficients from to P2 to P5−P8 are −8.94 dB, −9.46 dB, −8.84 dB and −10.08 dB, respectively. Fig. 13 illustrates the simulated phase differences between two adjoining output ports ($\angle S_{6p} - \angle S_{5p}$, $\angle S_{7p} - \angle S_{6p}$ and $\angle S_{8p} - \angle S_{7p}$), denoted as p corresponding to the number of P1–P4. The theoretical relative phase differences between these output ports are −45°, 135°, −135°, and 45°, respectively, when P1–P4 is excited.

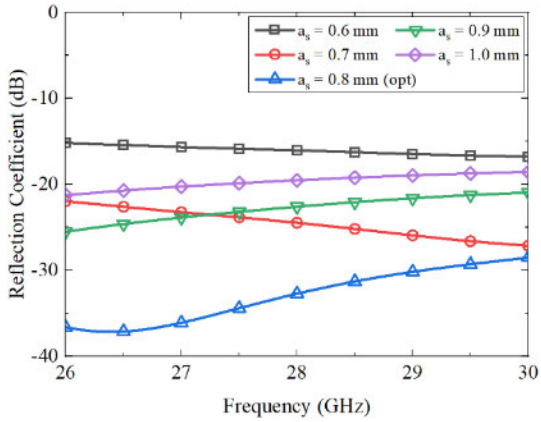

FIGURE 11. Simulated reflection coefficients at different width of anti-pad (α_S).

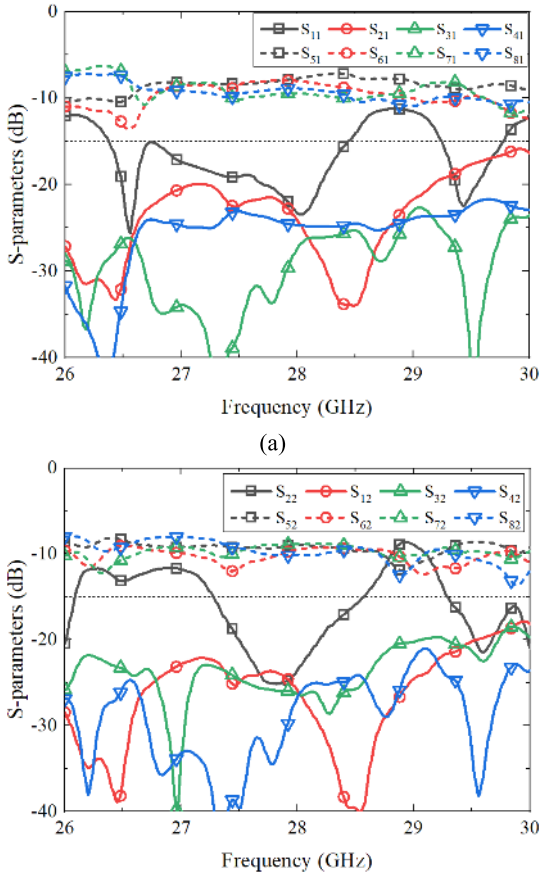

FIGURE 12. Simulated S-parameters results of the staked 4 × 4 Butler matrix. (a) S-parameter with P1 excited. (b) S-parameter with P2 excited.

Table 1 summarizes the simulated results. Comparing the theoretical relative phase difference with simulated phase difference, maximum phase error of −3.67°, 8.88°, −8.88°, and −3.67°, when p is 1, 2, 3 and 4, respectively.

Each single-patch antenna is realized using an LTCC-based microstrip line technology and is carefully designed with

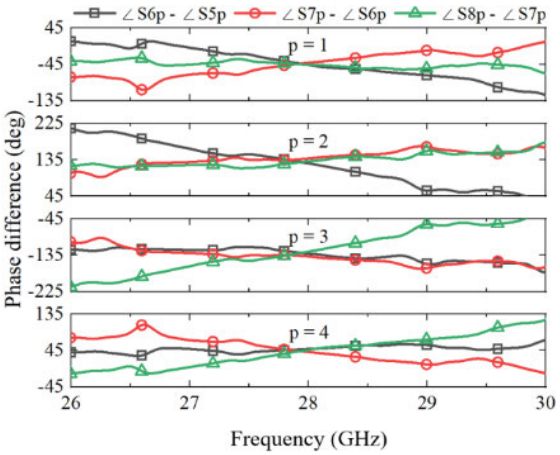

FIGURE 13. Simulated output phase differences (p = 1, P1 excited), (p = 2, P2 excited), (p = 3, P3 excited), (p = 4, P4 excited).

TABLE 1. Simulated output phase differences of the stacked 4 × 4 Butler matrix.

	$\angle S_{6p} - \angle S_{5p}$	$\angle S_{7p} - \angle S_{6p}$	$\angle S_{8p} - \angle S_{7p}$
p = 1	–46.32°	–41.33°	–45.76°
p = 2	126.12°	138.10°	131.27°
p = 3	–131.27°	–138.10°	–126.12°
p = 4	45.76°	41.33	46.32°

optimized parameters, as shown in Fig. 14 and detailed in Table 2. The power is transferred from the Butler matrix to the patch antenna through the through-via, with an anti-pad. Due to the high permittivity of LTCC, the input impedance at the edge of the patch is inherently high. To address this, an inset feed technique is employed, where the patch antenna is fed near its center with a distance of d_p from the patch end. The influence of the inset feed position on the reflection coefficient of the single-patch antenna is demonstrated in Fig. 15. It is observed that when the d_p is set to 0.74 mm, the reflection coefficient remains below than −20 dB at 28 GHz. Finally, each single-patch antenna is connected to the corresponding output of the 4 × 4 stacked Butler matrix, completing the integration of the Butler matrix antenna module, as illustrated in Fig. 16. Note that the spacing between the patch elements is set to half the wavelength in free space.

Before proceeding with the measurement results, it is worthy to investigate the spurious radiation. Fig. 17 illustrates 4 × 1 array patch antennas based on three different types of the Butler matrix. As depicted in Fig. 17(a), the Butler matrix is composed of microstrip on the same layer as the patch antennas. Fig. 17(b) shows a patch array antenna utilizing a stripline-based Butler matrix, which maintains a comparable size to the microstrip-based Butler matrix antenna. In contrast, the proposed design is a patch array antenna based on a stacked Butler matrix, as shown Fig 17(c), significantly reducing its length in the y-direction. The simulated radiation patterns of the three Butler matrix antennas are examined

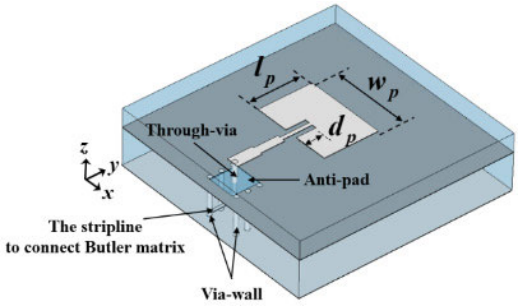

FIGURE 14. Structure of the single patch antenna based on LTCC.

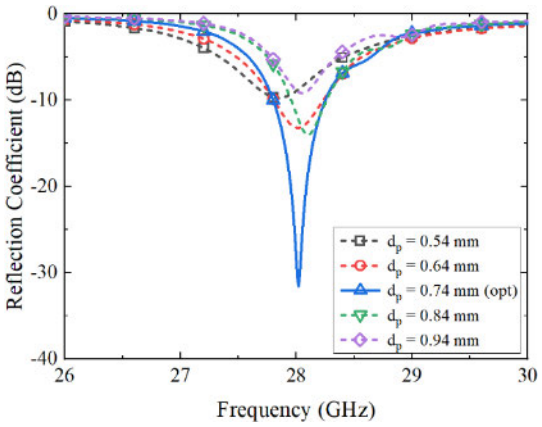

FIGURE 15. Simulated reflection coefficients depending on the position of the inset feed (d_p).

TABLE 2. Dimensions of the all components.

Parameter	Dimension [mm]	Parameter	Dimension [mm]
a_H	0.21	w_C	0.10
b_H	1.02	a_d	0.10
c_H	0.84	b_d	2.03
w_H	0.10	c_d	0.37
h_H	0.225	a_s	0.80
a_C	0.21	$\emptyset d_s$	0.15
b_C	0.98	w_p	2.60
c_C	0.89	l_p	1.79
d_C	0.38	d_p	0.74

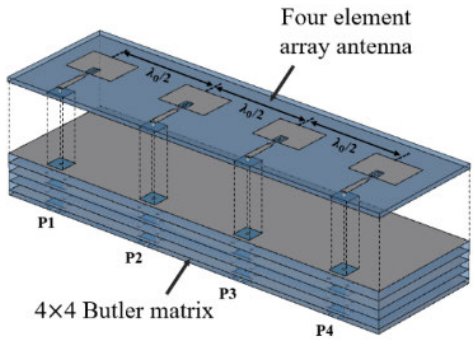

FIGURE 16. Structure of the array patch antenna with stacked 4 × 4 Butler matrix antenna.

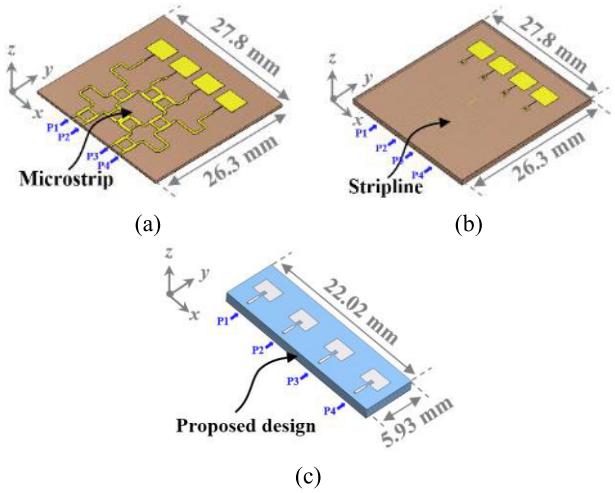

FIGURE 17. Three types of Butler matrix antenna. (a) Microstrip-based design. (b) Stripline-based design. (c) Proposed design.

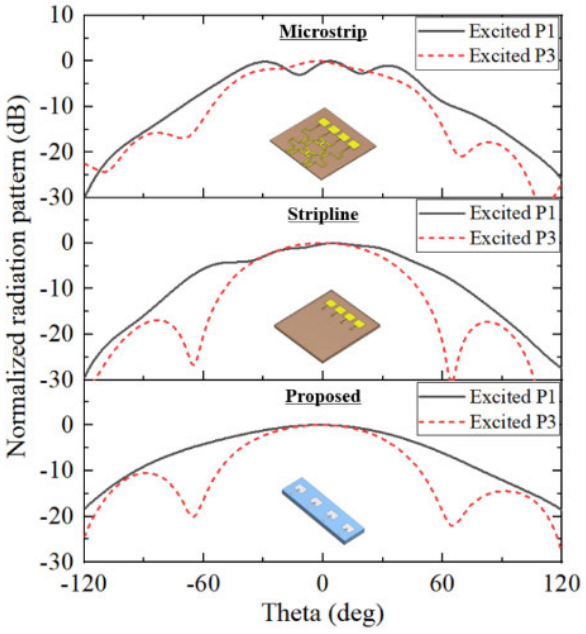

FIGURE 18. The simulated radiation patterns of the three different Butler matrix antennas.

in the y–z plane, as shown in Fig. 18. The microstrip-based Butler matrix antenna exhibits a non-flat main lobe with increased side lobes when both P1 and P3 are excited. This phenomenon is attributed to the radiation energy emitted from the Butler matrix, which is exposed to the surrounding air and interferes with the radiation pattern formed by the patch antennas. In addition, the stripline-based Butler matrix antenna form a flatter beam pattern due to the Butler matrix being buried under the conductor. However, it still exhibits an asymmetry in the main lobe when P1 is excited. This uneven main lobe may introduce beam pointing errors and results in a loss of gain. On the other hand, the proposed Butler matrix antenna with the stacked Butler matrix generally maintains a flat main lobe when each port is excited. This design effectively mitigates the spurious radiation effects observed in the conventional configurations. Thus, the proposed Butler matrix antenna provides a viable solution for enhancing radiation performance and achieving compact antenna designs by unwanted spurious radiation.

III. MEASUREMENT & VERIFICATION

A fabricated prototype of the 4 × 4 Butler matrix antenna was manufactured using the LTCC process. The dimensions of the fabricated prototype are 22.02 mm × 5.93 mm with a height of 1.20 mm, as shown in Fig. 19(a) and (b). For measurement purpose, the fabricated prototype is assembled on a dedicated test board, as depicted in Fig. 19(c). The test board consists of a TLY-5A with a dielectric constant of 2.17 and a loss tangent of 0.0009 and has four transmission lines with a characteristic impedance of 50 Ω to feed signals to the prototype. The input ports are connected to 2.92 mm end-launch connectors through extended transmission lines. To ensure accurate measurements, when an input signal is excited on one port, the remaining three ports are properly terminated with 50 Ω terminators.

Fig. 20 shows the simulated and measured reflection coefficients of the proposed 4 × 4 butler matrix antenna. As observed, with the P1 excited, the measured reflection coefficient is consistently below −15 dB within the frequency range of 25.7 GHz to 28.1 GHz. In addition, both the measured reflection coefficients with P2 excited and with P3 excited are less than −15 dB between 27.9 GHz and 28.4 GHz. Similarly, with the P4 excited, the measured reflection coefficient remains below −15 dB from

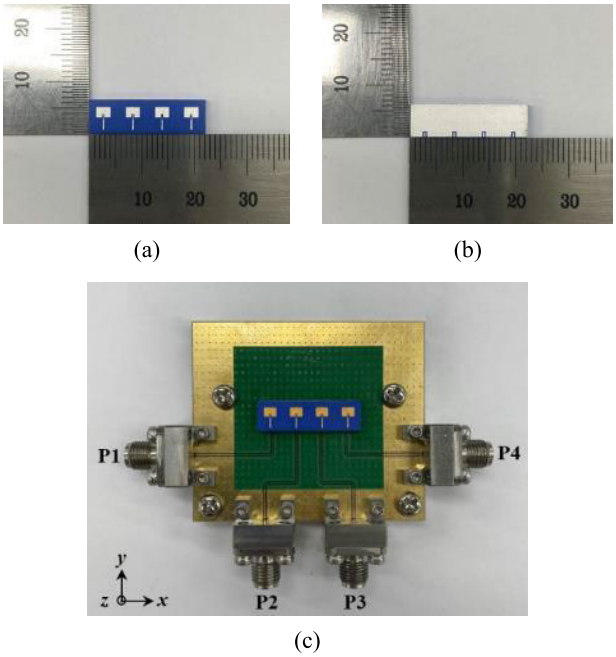

FIGURE 19. The fabricated array patch antenna with stacked 4 × 4 Butler matrix. (a) Top view. (b) Bottom view. (c) Test board.

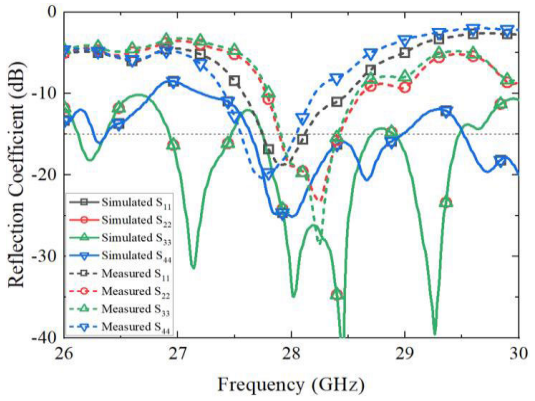

FIGURE 20. Simulated and measured reflection coefficient.

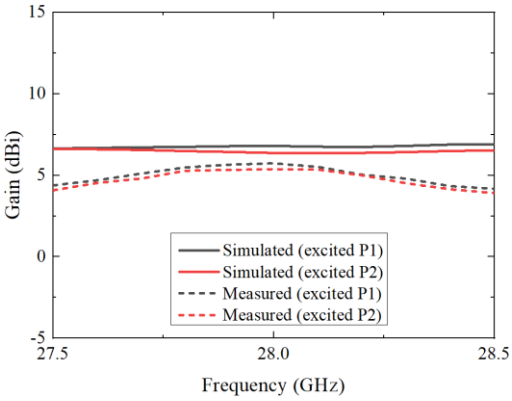

FIGURE 22. Simulated and measured gain of the proposed Butler matrix antenna.

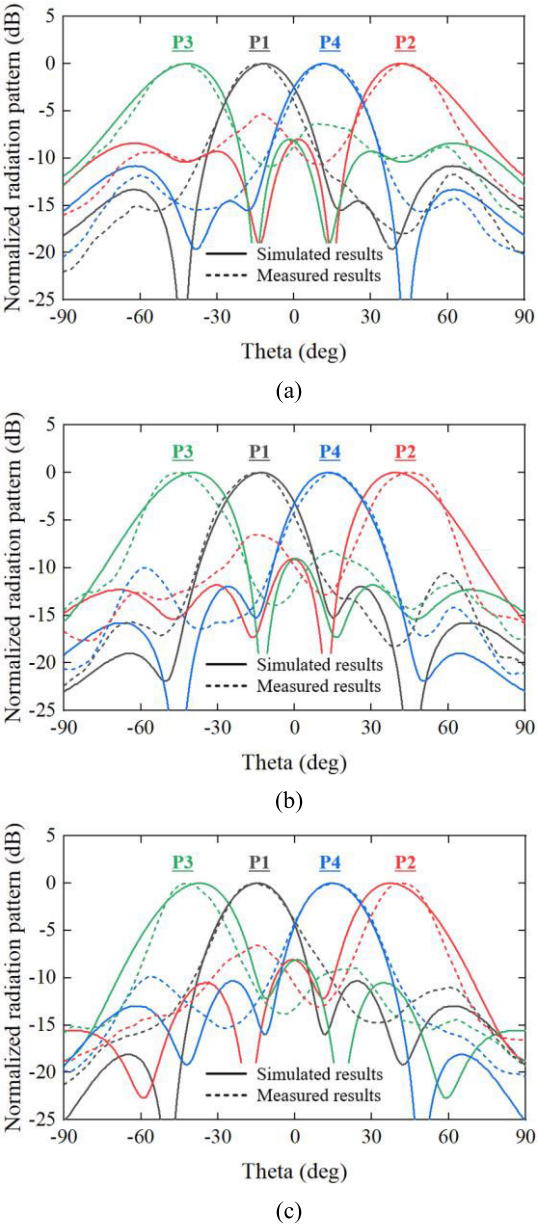

FIGURE 21. Simulated and measured normalized radiation patterns on the x–z plane. (a) f = 27.5 GHz. (b) f = 28.0 GHz. (c) f = 28.5 GHz.

27.5 GHz to 28.1 GHz. However, there are slight discrepancies between the simulated and measured results, primarily attributed to fabrication and measurement errors.

The radiation pattern of the fabricated prototype was evaluated in an anechoic chamber. Fig. 21 provides a comparative analysis of the normalized radiation patterns between simulation and measurement for the fabricated Butler matrix antenna. These comparisons are made at three distinct frequencies: 27.5 GHz, 28 GHz, and 28.5 GHz, with different input ports (P1−P4) being fed. Notably, the four beams exhibit the capability to cover a broad azimuthal range, roughly spanning ±45°. Furthermore, the measured results indicate that beams are generated with peak angles of −16°, 45°, −45°, and 16° at 28 GHz. In Fig. 22, we present the simulated and measured gain versus frequency when P1 or P2 is used as a feed input. The gain of the other ports is similar due to the symmetrical geometry of the structure. The measured peak gains of P1 and P2 are 5.73 dBi and 5.37 dBi, respectively, at 28 GHz. Some discrepancies between measured and simulated results may be attributed to manufacturing errors, material composition, measurement inaccuracies, and simulation inconsistencies.

Table 3 provides a comparative analysis of our research with previous studies on Butler matrix-based beamforming antenna systems. Much of the literature discusses single-layer or dual-layer Butler matrix antennas. They are constructed using PCB processes and thus integrated modules with Butler matrix and array antennas utilizing four or more layers remains under-explored [18], [20], [28], [30], [31], [32]. On the other hand, [33], [34], and [35] detail the creation of a Butler matrix with four or more layers using the LTCC process. The maximum beam steering angle and gain level compared to the number of antenna arrays in this work were similar or slightly worse than other studies using the LTCC process. Nevertheless, the proposed Butler matrix antenna is closely aligned with the theoretical beam scanning angle, and the gain discrepancy at the scanning-providing angle is under 0.5 dB. As such, these results are practically adequate for the demands of 5G mm-wave wireless systems. The focus of our study being on miniaturization, the comparative size

TABLE 3. Comparison of Butler matrix antennas.

Ref.	Freq (GHz)	Layer structure	Process	Butler matrix (antenna array)	Circuit size (mm)	Beam scanning (deg)	Peak gain (dBi)	Normalized size factor †
[18]	60	Single-layer	PCB	4 × 4 (1 × 4)	9.75 × 13.1 ($2.0\lambda_0 \times 2.6\lambda_0$)	–40 ~ 40	8.9	1.28
[20]	28	Single-layer	PCB	4 × 6 (1 × 6)	60.0 × 49.3 ($5.6\lambda_0 \times 4.6\lambda_0$)	–45 ~ 45	10.7	6.44
[28]	28	Dual-layer	PCB	4 × 4 (1 × 4)	86.7 × 50.8 ($8.1\lambda_0 \times 4.7\lambda_0$)	–42 ~ 42 *	11.1	9.61
[30]	3.5	Dual-layer	PCB	4 × 4 (1 × 4)	184.3 × 146.6 ($2.2\lambda_0 \times 1.7\lambda_0$)	–50 ~ 50	10.0	0.92
[31]	2.35	Dual-layer	PCB	4 × 4 (1 × 4)	280.0 × 260.0 ($2.2\lambda_0 \times 2.0\lambda_0$)	–40 ~ 40	6.1	1.12
[32]	30	Dual-layer	PCB	4 × 4 (2 × 4)	110.3 × 42.5 ($11.0\lambda_0 \times 4.3\lambda_0$)	–51 ~ 51	12.0	11.74
[33]	28	Stacked multilayer	LTCC	4 × 4 (1 × 4)	14.0 × 20.0 ($1.3\lambda_0 \times 1.9\lambda_0$)	–44 ~ 44	5.0	0.61
[34]	60	Stacked multilayer	LTCC	4 × 4 (1 × 4)	14.0 × 13.0 ($2.8\lambda_0 \times 2.6\lambda_0$)	–30 ~ 25	8.7	1.82
[35]	60	Stacked multilayer	LTCC	4 × 4 (4 × 4)	16.5 × 14.6 ($5.6\lambda_0 \times 4.0\lambda_0$)	–45 ~ 45	15.3	2.41
This work	28	Stacked multilayer	LTCC	4 × 4 (1 × 4)	22.0 × 5.9 ($2.0\lambda_0 \times 0.5\lambda_0$)	–45 ~ 45	5.7	0.28

† Calculated by total area / ($\lambda_0{}^2$ × beam direction count) in which λ_0 is the free-space wavelength.
* Simulated results

factor is crucial. To ensure consistency in our comparison, we adopted the normalized size factor as described in [26], which entails dividing the footprint area by the product of the square of the free space wavelength and the beam steering count. Our work achieves a size factor of 0.28, marking it as the most compact among Butler matrix antenna modules in existing literature.

IV. CONCLUSION

The proposed stacked 4 × 4 Butler matrix antenna presents a compact and efficient solution for 5G wireless applications. By vertically stacking the elements of the Butler matrix and the array antenna using the LTCC process, the size of the Butler matrix is significantly miniaturized, resulting in a compact overall antenna size of 22.02 × 5.93 × 1.20 mm^3, (2.056 λ_0 × 0.554 λ_0 × 0.112 λ_0). This stacked structure also significantly alleviates spurious radiation effects, enhancing the antenna's performance. The fabricated prototype demonstrated effective beam steering capabilities, enabling radiation beam scanning within angles of −16°, 45°, −45°, and 16°. These results validate the feasibility and effective-ness of the proposed stacked 4 × 4 Butler matrix antenna. Its compact size and beam scanning capabilities make it highly suitable for space-limited 5G applications, where size constraints are critical.

REFERENCES

[1] J. Temga, K. Edamatsu, M. Motoyoshi, and N. Suematsu, "A compact 28 GHz-band 4 × 4 Butler matrix based beamforming antenna module in broadside coupled stripline," in *Proc. 15th Eur. Conf. Antennas Propag. (EuCAP)*, Mar. 2021, pp. 1–4.

[2] T. Joo, C. Hwang, J. Park, K. Kim, and J. Jung, "Design of a tile-type Rx multi-beam digital active phased array antenna system," *J. Electromagn. Eng. Sci.*, vol. 22, no. 1, pp. 12–20, Jan. 2022.

[3] W. Hong, Z. H. Jiang, C. Yu, J. Zhou, P. Chen, Z. Yu, H. Zhang, B. Yang, X. Pang, M. Jiang, Y. Cheng, M. K. T. Al-Nuaimi, Y. Zhang, J. Chen, and S. He, "Multibeam antenna technologies for 5G wireless communications," *IEEE Trans. Antennas Propag.*, vol. 65, no. 12, pp. 6231–6249, Dec. 2017.

[4] A. Gupta and R. K. Jha, "A survey of 5G network: Architecture and emerging technologies," *IEEE Access*, vol. 3, pp. 1206–1232, 2015.

[5] R. J. Mailloux, "Antenna array architecture," *Proc. IEEE*, vol. 80, no. 1, pp. 163–172, Jan. 1992.

[6] T. Varum, A. Ramos, and J. N. Matos, "Planar microstrip series-fed array for 5G applications with beamforming capabilities," in *IEEE MTT-S Int. Microw. Symp. Dig.*, Aug. 2018, pp. 1–3.

[7] J.-H. Kim, J.-H. Han, J.-S. Park, and J.-G. Kim, "Design of phased array antenna for 5G mm-wave beamforming system," in *Proc. IEEE 5th Asia–Pacific Conf. Antennas Propag. (APCAP)*, Kaohsiung, Taiwan, Jul. 2016, pp. 201–202.

[8] F. W. Vook, A. Ghosh, and T. A. Thomas, "MIMO and beamforming solutions for 5G technology," in *IEEE MTT-S Int. Microw. Symp. Dig.*, Jun. 2014, pp. 1–4.

[9] L. Zhou, J. J. P. C. Rodrigues, H. Wang, M. Martini, and V. C. M. Leung, "5G multimedia communications: Theory, technology, and application," *IEEE MultimediaMag.*, vol. 26, no. 1, pp. 8–9, Jan. 2019.

[10] N. O. Parchin, M. Alibakhshikenari, H. J. Basherlou, R. A. Abd-Alhameed, J. Rodriguez, and E. Limiti, "MM-wave phased array Quasi–Yagi antenna for the upcoming 5G cellular communications," *Appl. Sci.*, vol. 9, no. 5, p. 978, Mar. 2019.

[11] F. Casini, R. V. Gatti, L. Marcaccioli, and R. Sorrentino, "A novel design method for Blass matrix beam-forming networks," in *Proc. Eur. Microw. Conf.*, Oct. 2007, pp. 232–235.

[12] P. Chen, W. Hong, Z. Kuai, and J. Xu, "A double layer substrate integrated waveguide Blass matrix for beamforming applications," *IEEE Microw. Wireless Compon. Lett.*, vol. 19, no. 6, pp. 374–376, Jun. 2009.

[13] F. E. Fakoukakis and G. A. Kyriacou, "Novel Nolen matrix based beamforming networks for series-fed low SLL multibeam antennas," *Prog. Electromagn. Res. B*, vol. 51, pp. 33–64, 2013.

[14] H. Hong, H. Park, K. Lee, W. Lee, S. Jo, J. Yang, C. Park, H. Lee, and S. K. Hong, "Ka-band Rotman lens-based retrodirective beamforming system for wireless power transfer," *J. Electromagn. Eng. Sci.*, vol. 21, no. 5, pp. 391–398, Nov. 2021.
[15] Y. J. Cheng, W. Hong, K. Wu, Z. Q. Kuai, C. Yu, J. X. Chen, J. Y. Zhou, and H. J. Tang, "Substrate integrated waveguide (SIW) Rotman lens and its Ka-band multibeam array antenna applications," *IEEE Trans. Antennas Propag.*, vol. 56, no. 8, pp. 2504–2513, Aug. 2008.
[16] N. M. Jizat, N. Ahmad, Z. Yusoff, N. M. Nor, and M. I. Sabran, "5G beam-steering 2 × 2 Butler matrix with slotted waveguide antenna array," *Telecommun. Comput. Electron Control. (Telkomnika)*, vol. 17, no. 4, pp. 1656–1662, Aug. 2019.
[17] S. Trinh-Van, J. M. Lee, Y. Yang, K.-Y. Lee, and K. C. Hwang, "A sidelobe-reduced, four-beam array antenna fed by a modified 4 × 4 Butler matrix for 5G applications," *IEEE Trans. Antennas Propag.*, vol. 67, no. 7, pp. 4528–4536, Jul. 2019.
[18] C.-H. Tseng, C.-J. Chen, and T.-H. Chu, "A low-cost 60-GHz switched-beam patch antenna array with Butler matrix network," *IEEE Antennas Wireless Propag. Lett.*, vol. 7, pp. 432–435, 2008.
[19] T.-H. Lin, S.-K. Hsu, and T.-L. Wu, "Bandwidth enhancement of 4 × 4 Butler matrix using broadband forward-wave directional coupler and phase difference compensation," *IEEE Trans. Microw. Theory Techn.*, vol. 61, no. 12, pp. 4099–4109, Dec. 2013.
[20] M. Ansari, H. Zhu, N. Shariati, and Y. J. Guo, "Compact planar beamforming array with endfire radiating elements for 5G applications," *IEEE Trans. Antennas Propag.*, vol. 67, no. 11, pp. 6859–6869, Nov. 2019.
[21] A. Bekasiewicz and S. Koziel, "Low-cost unattended design of miniaturized 4 × 4 Butler matrices with nonstandard phase differences," *Sensors*, vol. 21, no. 3, p. 851, Jan. 2021.
[22] G. S. Karthikeya, S. K. Koul, A. K. Poddar, and U. L. Rohde, "Compact bent-corner orthogonal beam switching antenna module for 5G mobile devices," *J. Electromagn. Eng. Sci.*, vol. 22, no. 1, pp. 74–83, Jan. 2022.
[23] E. Gandini, M. Ettorre, R. Sauleau, and A. Grbic, "A lumped-element unit cell for beam-forming networks and its application to a miniaturized Butler matrix," *IEEE Trans. Microw. Theory Techn.*, vol. 61, no. 4, pp. 1477–1487, Apr. 2013.
[24] Zulfi and A. Munir, "Experimental characterization of miniaturized meander line-based 4 × 4 Butler matrix," in *Proc. IEEE Int. Conf. Commun., Netw. Satell. (COMNETSAT)*, Jul. 2021, pp. 258–262.
[25] Z. M. Razi and P. Rezaei, "A two-layer beam-steering array antenna with 4 × 4 modified Butler matrix fed network for switched beam application," *Int. J. RF Microw. Comput.-Aided Eng.*, vol. 30, no. 2, Feb. 2020, Art. no. e22028.
[26] S. Kim, S. Yoon, Y. Lee, and H. Shin, "A miniaturized Butler matrix based switched beamforming antenna system in a two-layer hybrid stackup substrate for 5G applications," *Electronics*, vol. 8, no. 11, p. 1232, Oct. 2019.
[27] N. M. Jizat, Y. O. Yamada, and Z. Yusoff, "Radiation pattern of array antenna with the dual-layer Butler matrix," in *Proc. IEEE Int. RF Microw. Conf. (RFM)*, Dec. 2020, pp. 1–4.
[28] S. Dey, N. S. Kiran, and S. Dey, "SIW Butler matrix driven beam scanning array for millimeter wave 5G communication," in *Proc. IEEE Asia–Pacific Microw. Conf. (APMC)*, Dec. 2020, pp. 709–711.
[29] A. A. M. Ali, N. J. G. Fonseca, F. Coccetti, and H. Aubert, "Design and implementation of two-layer compact wideband Butler matrices in SIW technology for Ku-band applications," *IEEE Trans. Antennas Propag.*, vol. 59, no. 2, pp. 503–512, Feb. 2011.
[30] P. I. Bantavis, C. I. Kolitsidas, T. Empliouk, M. Le Roy, B. L. G. Jonsson, and G. A. Kyriacou, "A cost-effective wideband switched beam antenna system for a small cell base station," *IEEE Trans. Antennas Propag.*, vol. 66, no. 12, pp. 6851–6861, Dec. 2018.
[31] F. Y. Zulkifli, N. Chasanah, Basari, and E. T. Rahardjo, "Design of Butler matrix integrated with antenna array for beam forming," in *Proc. Int. Symp. Antennas Propag. (ISAP)*, Nov. 2015, pp. 1–4.
[32] Q.-L. Yang, Y.-L. Ban, J.-W. Lian, Z.-F. Yu, and B. Wu, "SIW Butler matrix with modified hybrid coupler for slot antenna array," *IEEE Access*, vol. 4, pp. 9561–9569, 2016.
[33] S. Nam, S. Choi, J. Ryu, and J. Lee, "Compact 28 GHz folded Butler matrix using low-temperature co-fired ceramics," *J. Electromagn. Eng. Sci.*, vol. 22, no. 4, pp. 452–458, Jul. 2022.
[34] H. Chu, Y.-X. Guo, and Z. Wang, "60-GHz LTCC wideband vertical off-center dipole antenna and arrays," *IEEE Trans. Antennas Propag.*, vol. 61, no. 1, pp. 153–161, Jan. 2013.
[35] Y. J. Cheng, X. Y. Bao, and Y. X. Guo, "60-GHz LTCC miniaturized substrate integrated multibeam array antenna with multiple polarizations," *IEEE Trans. Antennas Propag.*, vol. 61, no. 12, pp. 5958–5967, Dec. 2013.

JAEWOONG JUNG received the B.S. degree in electronic and electrical engineering from Dankook University, Gyeonggi-do, South Korea, in 2019. He is currently pursuing the M.S. degree in electronic engineering with Hanyang University, Seoul, South Korea. His current research interest includes design of array antenna for next generation wireless communication systems.

JONGIN RYU (Member, IEEE) received the B.S. and M.S. degrees in radio science and engineering and the Ph.D. degree in electronic engineering from Hanyang University, Seoul, South Korea, in 1998, 2000, and 2019, respectively. From 2002 to 2006, he was with Samsung Electronics, where he had developed the RF/modem IC application for GSM/GPRS/EDGE. In 2006, he joined the Korea Electronics Technology Institute (KETI). He has performed the development of the component of cell phone, including FEM, dual-band PAM, LTCC module, radar, and antennas. He focuses on researching on the array antennas and antenna-on-package module based on both LTCC and organic substrate.

KYUNG-YOUNG JUNG (Senior Member, IEEE) received the B.S. and M.S. degrees in electrical engineering from Hanyang University, Seoul, South Korea, in 1996 and 1998, respectively, and the Ph.D. degree in electrical and computer engineering from The Ohio State University, Columbus, OH, USA, in 2008.

From 2008 to 2009, he was a Postdoctoral Researcher with The Ohio State University. From 2009 to 2010, he was an Assistant Professor with the Department of Electrical and Computer Engineering, Ajou University, Suwon, South Korea. Since 2011, he has been with Hanyang University, where he is currently a Professor with the Department of Electronic Engineering. His current research interests include computational electromagnetics, bioelectromagnetics, and nanoelectromagnetics.

Dr. Jung was a recipient of the Graduate Study Abroad Scholarship from the National Research Foundation of Korea, the Presidential Fellowship from The Ohio State University, the HYU Distinguished Teaching Professor Award from Hanyang University, and the Outstanding Research Award from the Korean Institute of Electromagnetic Engineering and Science.